Journal of Advanced Research 76 (2025) 715–729

Contents lists available at ScienceDirect

Journal of Advanced Research

journal homepage: www.elsevier.com/locate/jare

Original Manuscript

LTX-315 is a novel broad-spectrum antimicrobial peptide against clinical multidrug-resistant bacteria

Yang Tang [a,b], Chen Yang [a,b], Jiamin Zhao [b], Heng Heng [a,b], Mingxiu Peng [c], Liang Sun [d], Liang Dai [e], Edward Wai-Chi Chan [b], Sheng Chen [b,c,*]

[a] Department of Infectious Diseases and Public Health, Jockey Club College of Veterinary Medicine and Life Sciences, City University of Hong Kong, Kowloon, Hong Kong
[b] State Key Laboratory of Chemical Biology and Drug Discovery and the Department of Food Science and Nutrition, The Hong Kong Polytechnic University, Hung Hom, Kowloon, Hong Kong
[c] Shenzhen Key Laboratory for Food Biological Safety Control, Food Safety and Technology Research Centre, The Hong Kong PolyU Shenzhen Research Institute, Shenzhen, PR China
[d] City University of Hong Kong, Shenzhen Research Institute, Nanshan, PR China
[e] Department of Physics, City University of Hong Kong, Kowloon, Hong Kong

HIGHLIGHTS

- LTX-315 exhibits broad-spectrum antibacterial activity and demonstrates low resistance development.
- It is effective in a mouse model infected with hypervirulent and multidrug-resistant *Klebsiella pneumoniae*.
- The alkyl chain's hydrophobicity boosts the indole group's ability to recognize and bind with the phosphate anion of PG.
- Its strong activity and broad bacterial coverage suggest potential as an antimicrobial agent against rising resistance.

GRAPHICAL ABSTRACT

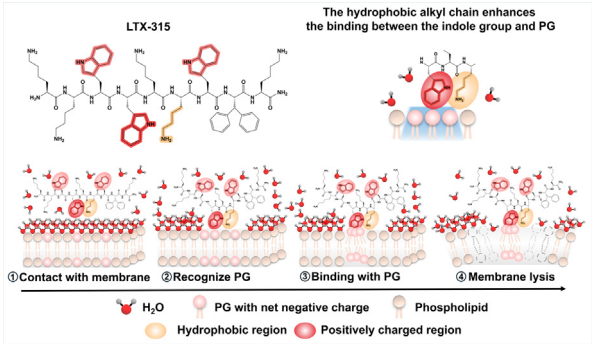

ARTICLE INFO

Article history:
Received 17 October 2024
Revised 17 December 2024
Accepted 28 December 2024
Available online 9 January 2025

Keywords:
Antimicrobial resistance
Bactericidal effect
Antimicrobial peptide
Broad spectrum

ABSTRACT

Introduction: Infections stemming from multidrug-resistant bacteria present a substantial threat to public health today. Discovering or synthesizing novel compounds is crucial to alleviate this pressing situation.
Objective: The main purpose of this study is to verify the antibacterial activity of LTX-315 and explore its primary action mode.
Methods: Through antibacterial phenotype assay screening, we obtained a potent compound named LTX-315 from diverse drug libraries, 10,926 compounds in total. Then, the bactericidal effect and its action mode were explored through biochemical and chemistry methods such as a time-killing curve, scanning electronic microscopy, isothermal titration calorimetry analysis, and nuclear magnetic resonance. Finally, the efficacy in vivo of LTX-315 against drug-resistant bacteria was proved through a mice infection model.
Results: In this study, LTX-315, an oncolytic peptide, was discovered to effectively eliminate gram-positive and gram-negative pathogens, even for those multidrug-resistant strains. Through strong electrostatic interactions, LTX-315 can bind to the membrane component phosphatidylglycerol (PG) with extremely high affinity (nanomolar level). Strikingly, in contrast to the typical electrostatic interactions

* Corresponding author at: State Key Laboratory of Chemical Biology and Drug Discovery and the Department of Food Science and Nutrition, The Hong Kong Polytechnic University, Hung Hom, Kowloon, Hong Kong.
E-mail address: sheng.chen@polyu.edu.hk (S. Chen).

https://doi.org/10.1016/j.jare.2024.12.044
2090-1232/

of antibacterial peptides, the indole group of LTX-315, situated near the alkyl chain, exhibits significantly enhanced recognition and interaction with PG due to the hydrophobic effect of the alkyl chain. Furthermore, it exerts various impacts on cell membranes, including damaging integrity, increasing permeability, and decreasing membrane fluidity. Additionally, microscopy revealed significant cell disintegration. The influence, in turn, disrupts several physiological activities inside cells, such as increasing the reactive oxygen species level, ultimately leading to cell death. Finally, the efficacy of LTX-315 in vivo against multidrug-resistant and hypervirulent *Klebsiella pneumoniae* was demonstrated.

Conclusion: The unique mechanism of LTX-315 involves high-affinity binding to PG and subsequent membrane disruption, providing a novel approach against multidrug-resistant bacteria compared to conventional antibiotics. As a potential candidate, it shows promise in effectively treating bacterial infections, particularly those caused by drug-resistant bacteria, thereby addressing the escalating challenge of antibiotic resistance worldwide.

Introduction

Bacteria are widely ubiquitous as prokaryotic organisms. They are commonly classified as either Gram-negative or Gram-positive based on Gram staining [1]. In the context of human health, certain bacteria known as probiotics can be beneficial. For example, lactic acid bacteria (LAB) play a crucial role in microbiota in the human gut; specific strains can produce compounds that combat pathogens like yeast and fungi [2]. However, bacteria such as *Escherichia coli*, *Klebsiella pneumoniae*, *Acinetobacter baumannii,* and *Staphylococcus aureus* pose significant threats to public health. Strains like carbapenem-resistant Enterobacterales, carbapenem-resistant *Acinetobacter baumannii* (CRAB), hypervirulent *K. pneumoniae* (Hvkp), and methicillin-resistant *S. aureus* (MRSA) are responsible for numerous human infections and even deaths worldwide [3–6]. Additionally, it is estimated that the economic loss caused by antibiotic resistance will reach approximately $300 billion by 2050 [7]. Beyond the financial burden, these bacterial infections also endanger lives, underscoring the urgent need to develop antibacterial materials.

The prolonged human lifespan owes much to the discovery of antibiotics during the golden age from the 1960s to the 1980s, which yielded well-known antibiotics like penicillin, polymyxin, and quinolones [8]. However, the escalating phenomenon of bacterial resistance to antibiotics due to their overuse and misuse in clinical settings is a growing concern [9]. The increase of multidrug-resistant bacteria poses a particularly alarming threat on a global scale. The problem of antimicrobial resistance is regarded as a critical human health issue that urgently needs to be addressed as a priority by the World Health Organization (WHO) [10]. Instances such as the evolution of hypervirulent *Klebsiella pneumoniae* strains, which have recently became multi-resistant to antibiotics, highlight the severity of the issue[11]. Bacteria can develop resistance to antibiotics through various mechanisms. One common strategy is reducing the concentration of antibiotics inside the cell which can occur by decreasing membrane permeability or actively expelling antibiotics using efflux pumps [12]. Another approach involves blocking the interaction between antibiotics and their targets, which may result from genetic mutations or modifications that alter the target site, rendering the antibiotic ineffective. Additionally, bacteria can neutralize antibiotics by chemically modifying or breaking them down through enzymatic hydrolysis [13]. Resistance can also spread between bacteria via horizontal gene transfer, a process where genetic material is shared among different bacterial strains in the environment [14]. The rapid evolution of bacteria outpaces the development of effective treatments, emphasizing the need for new strategies or drugs to combat this situation [15].

Antimicrobial peptides (AMPs) have recently gained more attention as a new class of antimicrobial agents with broad clinical application prospects [16]. As a clinically used polymyxin, colistin can damage the out-membrane against Gram-negative pathogens such as *E. coli* and *K. pneumoniae* [17]. Thiopeptides can inhibit protein synthesis by binding with the subunit of Gram-negative ribosome to complete the killing effect [18]. When used in combination, the peptides of Esc (1–21) and colistin exhibit a substantial bactericidal effect against multidrug-resistant *A. baumannii*, whereas when administered individually, their impact is null [19]. Some antimicrobial peptides present high nephrotoxicity [20]. Despite significant progress, issues such as a narrow spectrum, limited potency, and cytotoxicity continue to impede their clinical development [16].

In this study, through screening diverse drug databases including 10,926 compounds, LTX-315, an oncolytic peptide developed initially to kill drug-resistant cancer cells [21], was proved to have potent bactericidal effects for bacteria regardless of whether they are Gram-positive or negative. The action mode, efficacy, and safety of LTX-315 make it a potential antibiotic to combat multidrug-resistant bacterial pathogens.

Materials and methods

Antimicrobial susceptibility test

For the screening process, the drug libraries included U.S. Food and Drug Administration-approved drugs, natural compounds, homology of medicine and food, and clinical compounds, 10,926 compounds in total (MCE, HY-L0001). The minimum inhibitory concentration (MIC) of tested compounds for the tested strains was detected based on the broth micro-dilution method of the Clinical and Laboratory Standards Institute (CLSI), which is the gold standard for susceptibility testing [22].

Mueller–Hinton II Broth (MHB, BD Medical Technology) was used for all the tests. Approximately 5×10^5 cells per ml of bacteria concentration was adjusted in this assay. The lowest concentration of invisible bacterial growth was determined as the MIC after incubation at 37 °C for 18 h. Supplementary Materials Table S1 contains this study's strain information. Information on clinical strains can be referenced in Chen and Zhang et al. for isolation [23–27]. Each experiment was biologically repeated three times.

For the detection of the MIC of LTX-315(T6881, TargetMol) within a certain pH range (5–10), the MHB was adjusted using sodium hydroxide or hydrochloric acid and determined by a pH meter (Mettler-Toledo, FE-28). Each experiment was biologically replicated three times.

Checkboard assay

Fractional inhibitory concentrations (FICs) were determined by following the description of Song et al [28]. To assess the tested

materials' influence on LTX-315, the tested materials were serially diluted in MH medium, and 100 μL of each dilution was dispensed into 96-well plates. Subsequently, an equal volume of the above medium containing LTX-315 was added to the first column. Doubling dilutions were performed in order, and approximately 5×10^5 cells per ml were seeded into each well. The observation was completed after being placed at 37 °C for 18 h. The MIC was determined to be the lowest concentration at which no visible bacterial growth was observed. The synergistic antimicrobial effect was determined by calculating the fractional inhibitory concentration (FIC) using the following formula:

FIC index = $MIC_{ab}/(MIC_a) + MIC_{ba}/(MIC_b) = FIC_a + FIC_b$ (1).

where MIC_a represents the MIC of compound a alone, MIC_b indicates the MIC of compound b alone, MIC_{ab} signifies the MIC of compound a observed in the presence of compound b, MIC_{ba} denotes the MIC of compound b observed in the presence of compound a, FIC_a represents the FIC of compound a, and FIC_b indicates the FIC of compound b. The evaluation criteria are shown in the attached figure.

The tested materials included lipids such as 1-palmitoyl-2-oleoyl-*sn*-glycero-3-phospho-(1′-*rac*-glycerol) (sodium salt) (PG, Avanti Polar Lipids, 840457P), 1-palmitoyl-2-oleoyl-*sn*-glycero-3-phosphoethanolamine (PE, Avanti Polar Lipids, 850757), Lipopolysaccharide (LPS, Sigma-Aldrich, L2880); cations like copper sulfate pentahydrate ($CuSO_4{\cdot}5H_2O$, Fisher Chemical, LC134051), potassium chloride (KCl, Fisher Chemical, P217-10), sodium chloride (NaCl, Fisher Chemical, S271-500), calcium chloride anhydrous ($CaCl_2$, Uni-chem, C08130-4I), zinc sulfate, manganese sulfate monohydrate ($MnSO_4{\cdot}H_2O$, Sigma-Aldrich, M7634), cobalt chloride ($CoCl_2$, Alfa Aesar, B22031), iron sulfate heptahydrate ($FeSO_4{\cdot}7H_2O$, Sigma-Aldrich, F7002), iron chloride hexahydrate ($FeCl_3{\cdot}6H_2O$, Sigma-Aldrich, 44944), magnesium sulfate ($MgSO_4$, Uni-chem, M06870-4I).

Time-Killing curve

The killing rate of LTX-315 for tested strains was determined through a time-killing curve adapted from the description by Ling et al [29]. Overnight bacteria cultures (*E. coli* 25922; MRSA 43300; Hvkp2) were diluted in fresh LB broth with a dilution factor 1:10,000. The strains were then immediately incubated at 37 °C, 250 rpm, for 2 h to reach the early exponential phase. Subsequently, the strains were challenged with different concentrations (1/4 × MIC to 2 × MIC) of LTX-315 based on the MIC results for each strain. Time points were set at 0, 1, 3, 5, 7, and 24 h. One hundred microliter aliquots were ten times serially diluted at each interval and plated on MH agar plates. After incubation at 37 °C overnight, colonies were counted. Each experiment was biologically replicated three times.

Resistance development studies

Spontaneous resistance strains of *E. coli* 25922 and MRSA 43300 against LTX-315 were detected based on methods described by Ling et al [29]. Briefly, 1×10^9c.f.u. of *E. coli* 25922 and MRSA 43300 were plated onto MH agar containing 4 × MIC of LTX-315. The plates were then incubated at 37 °C for 48 h. No resistant colonies appeared for either of the two strains. Induced-resistance studies of LTX-315 for *E. coli* 25922 were performed in 1.5 mL Eppendorf tubes. Overnight cultured *E. coli* 25922 was incubated in tubes with 1 mL LB medium at a ratio of 1:100. The LTX-315 was added at different concentrations based on the MIC, doubled up to four times, and incubated at 37 °C overnight. The bacteria grown under the highest concentration were passaged, and relative concentrations of LTX-315 were added according to the MIC results of the tubes. The period was set for 30 days to determine the limit of its resistance degree. Generally, the MIC result in the tube slightly differed from the result of the broth micro-dilution method. Therefore, all grown-up strains were spread on an MH agar plate, and the broth micro-dilution method was used to detect the MIC of LTX-315. Colistin, as the last line against gram-negative infections with multidrug-resistant, served as a control in this study [30].

Cell contents leakage assays

Overnight culture of *E. coli* 25922 was diluted 1:100 in fresh LB broth and incubated at 37 °C, 250 rpm, till the OD_{600} reached 0.5. Then, centrifuged and washed the pellet thrice with phosphate-buffered saline (PBS, Thermo Scientific, 21600–044) to remove the medium residue entirely. The washed pellet was then resuspended and exposed to LTX-315 at concentrations of 1/2 × MIC, 1/4 × MIC, and 1/8 × MIC. Samples of 1 mL were collected at two-hour intervals over a total duration of eight hours. After centrifugation at 12,000 rpm for two minutes, the concentrations of DNA, RNA, and protein in the samples were measured using a Nanodrop Microvolume Spectrophotometer (Thermo Scientific, NanoDrop™ One). Each experiment was biologically replicated three times.

ONPG assay

After the action of the enzyme β-galactosidase, which is located inside the cell, O-Nitrophenyl-β-D-galactopyranoside (ONPG, Thermo Fisher, 34055) can be hydrolyzed into two components: galactose and o-nitrophenol [31]. Importantly, o-nitrophenol is yellow, indicating the progress of the reaction. Briefly, overnight culture strains (*E. coli* 25922, MRSA 43300) were seeded 1:100 in fresh LB broth and incubated at 37 °C with shaking at 250 rpm until the optical density at 600 nm (OD_{600}) reached approximately 0.6. They were then washed once and resuspended in saline. ONPG with a final concentration of 0.75 M was added and thoroughly mixed. Subsequently, 100 μL was added to each well, and the absorbance at 420 nm was measured for 5 min. Based on MIC results, LTX-315 was added at various concentrations, and the detection continued. The duration was set to 60 min. Each experiment was biologically replicated three times.

Membrane permeability detection

N-Phenyl-1-naphthylamine (NPN, Aladdin, P110559) was used to detect the effect of compounds on membrane permeability, with slight modifications according to the description by Lee et al [32]. In brief, 1 mL of resuspended cells was exposed to 1/2 × MIC LTX-315. The group treated with polymyxin B nonapeptide (PMBN, MCE, HY-106783) of 50 μg/mL, known to permeabilize bacterial outer membranes, was pointed as the positive control. In contrast, the untreated group was the negative control. The buffer contained 5 mM HEPES and 5 mM glucose (Fisher Scientific, MP21946721) at pH 7.2 to wash and resuspend the cells. Then NPN (final concentration of 4 μ M) was added to these samples, and the fluorescence value was measured under excitation at 350 nm and emission at 420 nm. All measurements were conducted using the CLARIOstar multimode microplate reader (BMG LABTECH). Each experiment was biologically replicated three times.

Membrane integrity detection

The impact of LTX-315 on the membrane integrity of *E. coli* 25922 was assessed using propidium iodide (PI, Thermo Scientific,

P1304MP), as detailed by Ma et al [33]. The overnight culture of the strain was diluted in fresh LB broth as a dilution factor of 1:100 and incubated at 37 °C, 250 rpm, until the OD_{600} reached 0.5. Following a single wash with PBS (pH 7.4), PI at a final concentration of 5 μM was added to a resuspended pellet in a buffer containing 5 mM HEPES (BioFroxx, EZ3455C330) and 5 mM glucose (Fisher Scientific, MP21946721) at pH 7.2. The culture was incubated in the dark for 30 min and then treated with various concentrations of -LTX-315 for another 30 min. The effect on membrane integrity was assessed by recording the fluorescence signal under excitation at 535 nm and emission at 615 nm. For kinetic analysis, the resuspended cells were monitored in a black plate for 5 min before exposure to LTX-315. The total incubation time was 60 min, and the detection conditions remained the same. The measurements were conducted using the CLARIOstar multimode microplate reader (BMG LABTECH). Each experiment was biologically replicated three times.

Membrane fluidity assays

Membrane fluidity is a crucial property for bacterial membranes to cope with environmental variations such as temperature or antibiotic pressure, and the measurement method was described by Wenzel et al [34]. Before the experiment, all materials, including tubes, plates, and 4 × Laurdan buffer, were prewarmed to 37 °C. Overnight bacteria cultures were incubated in fresh LB broth with a dilution factor of 1:100 until the OD_{600} reached 0.5. Laurdan was added and incubated for ten minutes at a final concentration of 10 μM. The cells were washed and resuspended in 4 × Laurdan buffer, ensuring gentle resuspension to avoid shearing forces. The cell density was adjusted to an OD_{600} of 0.4, and 200 μL was distributed into each well. An incubation with 30 mins at 37 °C was performed after adding LTX-315 with various concentrations (1/2 × MIC to 2 × MIC). Wells treated with benzyl alcohol at 30 mM, known to increase membrane fluidity, were pointed as the positive control, while untreated wells were the negative control. The measurements were conducted using the CLARIOstar multimode microplate reader under excitation at 350 nm and emission at 460 nm and 500 nm. The Laurdan GP, an index representing membrane fluidity, was calculated using the formula (2):

$$\text{Laurdan GP} = (I_{460} - I_{500}) / (I_{460} + I_{500}) \quad (2)$$

Where I_{460} represents the fluorescence value under excitation at 350 nm and emission at 420 nm, and I_{500} represents the fluorescence value under excitation at 350 nm and emission at 500 nm. Each experiment was biologically replicated three times.

Membrane potential assay

The membrane potential of bacteria was assessed using voltage-sensitive DiSC3(5) (Thermo Fisher, D306) [35]. An overnight culture of *E. coli* 25922 was incubated in fresh LB broth with a dilution factor of 1:100. After reaching an OD_{600} of 0.5, the culture was centrifuged, washed with saline, and the pellet was resuspended in saline. The OD_{600} was adjusted to 0.2, and KCl and DiSC3 (5) were added at final concentrations of 100 mM and 1 mM, respectively. The mixture was incubated in darkness for 15 min. Subsequently, 150 μL of the mixture was added to each well and then exposed to LTX-315 (1/2 × MIC) after a 30-minute incubation. Valinomycin at 5 mg/mL was pointed as the positive control, while the saline-treated group was the negative control. The fluorescence intensity was recorded at an excitation wavelength of 610 nm and an emission wavelength of 660 nm. Each experiment was biologically replicated three times.

Artificial Liposome-Calcein damage assay

The preparation of liposome-calcein and details followed the protocol and description of Dotta et al. and Chen et al [36,37]. Briefly, each well was distributed with 50 μL liposome-calcein mixture (1 mM). Then dimethyl sulfoxide (DMSO, Alfa Aesar) and Triton X-100 (2 μL each) were added as the solvent and positive control, respectively. LTX-315 stock was diluted to various concentrations and incubated with liposome-calcein (1 mM) for 10 min. Fluorescence signals were detected at excitation/emission wavelengths of 485/530 nm. Each experiment was biologically replicated three times.

ROS detection

The detection of reactive oxygen species (ROS) in bacteria was identical to Hu et al.'s description [38]. Overnight cultures of *E. coli* 25922 and MRSA 43300 were incubated in fresh LB broth with a dilution factor of 1:100. The cultures were then incubated at 37 °C and 250 rpm until the OD_{600} reached 0.6. CM-H2DCFDA was added to achieve a final concentration of 10 μM after washing with PBS (pH 7.4) once. The cultures were incubated at 37 °C for 30 min in the dark to allow dye penetration. The bacteria were centrifuged to remove the external dye, and the pellet was washed with PBS (pH 7.4) three times. The OD_{600} was adjusted to 0.3, and 200 μL was added to each well. The cells were then challenged with LTX-315 at relative concentrations. The untreated group was the negative control, while the treated group with 100 μM H_2O_2 was the positive control. Fluorescence signals were detected at excitation/emission wavelengths of 490/525 nm after a 30-minute incubation at room temperature. Each experiment was biologically replicated three times.

Hydrogen peroxide and peroxidase detection

Hydrogen peroxide and peroxidase activity were detected following the Amplex® Red Hydrogen Peroxide/Peroxidase Assay Kit (Thermo Scientific, A22188). Overnight cultures of *E. coli* 25922 and MRSA 43300 were incubated in fresh LB broth with a dilution factor of 1:100. After reaching an OD_{600} of 0.6 (37 °C, 250 rpm), the cultures were washed and resuspended in saline. The total system volume was 100 μL, containing 50 μL of the sample and 50 μL of the reaction buffer. Relative concentrations of LTX-315 were added to each well and incubated at room temperature for 30 min. For H_2O_2 detection, 0.2 U/mL HRP was prepared for the reaction buffer, while 2 mM H_2O_2 was prepared for peroxidase detection. For H_2O_2 detection, 10 μM H_2O_2 in 1X reaction buffer was pointed as the positive control, and 1X reaction buffer without H_2O_2 was the negative control. For peroxidase detection, 2 mU/mL HRP solution in reaction buffer was pointed as the positive control, while 1X negative buffer without HRP was the negative control. Finally, fluorescence signals were detected at excitation/emission wavelengths of 550/590 nm. The period was 180 min for kinetics detection, with readings taken every 30 min. Each experiment was biologically replicated three times.

NO assays

A sensitive probe for NO, DAF-FM, was used to measure NO amount in strains *E. coli* 25922 and MRSA 43300 [39]. Overnight cultures were diluted 1:100 in fresh LB broth and washed with saline once after reaching an OD_{600} of 0.5. DAF-FM was added to achieve a final concentration of 10 μM and incubated at 37 °C for 60 min. The bacteria were centrifuged, and the pellet was washed with saline three times. The OD_{600} was adjusted to 0.3, and the

strains were challenged with relative concentrations of LTX-315 for 30 min. The untreated group was pointed as the negative control. Fluorescence values were measured at excitation and emission wavelengths of 490 nm and 515 nm, respectively. Each experiment was biologically replicated three times.

•OH and $^{-}$OCl detection

3′-(p-aminophenyl) fluorescein (APF, Thermo Scientific, A36003) is relatively more sensitive to $^{-}$OCl, while 3′-(p-hydroxyphenyl) fluorescein (HPF, Thermo Scientific, H36004) is sensitive to •OH [40]. Briefly, overnight cultures of *E. coli* 25922 and MRSA 43300 were incubated in fresh LB broth with a dilution ratio 1:100. An OD_{600} of 0.6 was obtained, and the cultures were washed with PBS (pH 7.4) once. APF or HPF was added to achieve a final concentration of 10 μM, and the cultures were incubated at 37 °C and 250 rpm for 1 h. The bacteria were washed with PBS three times, and the OD was adjusted to 0.3. Subsequently, 200 μL of suspension was distributed into each well. The treated group received LTX-315 at various concentrations, while the untreated group was pointed as the negative control. Fluorescence signals were detected at excitation/emission wavelengths of 490/515 nm. Each experiment was biologically replicated three times.

ATP assays

The effect of LTX-315 on ATP levels in strains *E. coli* 25922 and MRSA 43300 was measured using the ATP detection kit (Thermo Scientific, A22066). Overnight cultures were diluted 1:100 in fresh LB medium. After reaching an OD_{600} of 0.6, the cultures were washed and resuspended in PBS (pH 7.4). The resuspension (OD_{600} = 0.5) was treated with various concentrations of LTX-315 for 30 min at 37 °C. The untreated group was pointed as the negative control. The cultures were centrifuged at 6,500 rpm for 5 min, and the supernatant was stored at 4 °C for extracellular ATP detection. The pellet was lysed using 200 μL of lysozyme (20 mg/mL) and lysostaphin (64 U/mL). All processes were performed on ice to minimize ATP degradation. The ATP reaction buffer was prepared by following the kit instructions. Then, 90 μL of reaction buffer was added to a white 96-well microplate and incubated for 5 min at room temperature. Subsequently, 10 μL of samples were added to each well and placed in the CLARIOstar to record luminescence at full wavelength. Each experiment was biologically replicated three times.

NAD/NADH assays

The NAD/NADH levels in strains *E. coli* 25922 and MRSA 43300 were determined using the NAD/NADH Assay Kit (BioAssay Systems, E2ND-100) [41]. Overnight cultures were diluted in fresh LB medium with a dilution factor of 1:100 and incubated at 37 °C, 250 rpm, until the OD_{600} reached 0.3. The cultures were divided into treated and control groups. The treated group was challenged with LTX-315 at 1/2 × MIC and incubated for 30 min at 37 °C. Then, it was incubated with the relevant detection buffer and detected optical density. Details can be seen in the description of Tang et al [37]. Each experiment was biologically replicated three times.

RNA sequencing and analysis

RNA was isolated for the tested strains using the RNeasy Mini Kit (QIAGEN, 74104). DNA was subsequently removed from the samples using the TURBO DNA-free Kit (Thermo Fisher, AM1907). The integrity and purity of the RNA samples were assessed with the Fragment Analyzer System (Agilent, 5400). Afterwards, rRNA was removed, and the mRNA library was constructed. Finally, sequencing was carried out on the NovaSeq 6000 Sequencing System (Illumina). For analysis, the RNA sequencing results were first mapped to the *E. coli* 25922 genome using HISAT2 (v2.2.1), followed by quantification with featureCounts (v2.0.6). Genes were annotated using eggNOG-mapper (2.1.12), and differential gene expression was analyzed using DESeq2 (v1.42.1) [42]. Genes with an adjusted p-value (P.adj) below 0.01 and an absolute log2 fold change exceeding 1 were considered significantly differentially expressed. Enrichment analyses for Gene Ontology (GO) and Kyoto Encyclopedia of Genes and Genomes (KEGG) pathways were conducted using clusterProfiler (v4.10.1). The variability of the replicates was assessed through Principal Component Analysis (PCA) using DESeq2 (v1.42.1).

NMR experiments

Approximately 2 mg of LTX-315 (acetate) was dissolved in 1 mL of D_2O, and NMR spectra were recorded on a Bruker Advance Neo 500 (^{1}H: 500 MHz; ^{13}C: 125 MHz) spectrometer at room temperature. To study the interaction between LTX-315 and PG or PE, different molar equivalents were mixed and analyzed under the same conditions. The following NMR experiments were performed on these samples: ^{1}H, ^{13}C, ^{1}H–^{1}H COSY, ^{1}H–^{1}H NOESY, and ^{1}H–^{13}C HSQC.

Isothermal titration calorimetry assay

To assess the binding affinity of LTX-315 to PG, isothermal titration calorimetry (ITC) was conducted. HEPES-NaCl (50:150 mM) was used as the reaction buffer throughout the assay. The PG to LTX-315 ratio was set at 1:5 (40 μM: 200 μM). Each reaction involved a 400 μL cell volume and a 150 μL titrant volume, with each titration drop measuring 1.9 μL. All experiments were conducted using the MicroCal automated Isothermal Titration Calorimeter (ITC, Malvern). Subsequently, the data on binding constants (K_d) and reaction stoichiometry (n) were analyzed and calculated utilizing relevant software.

Molecular dynamics

This study conducted molecular dynamics simulations of the POPG lipid-drug (LTX-315) system using GROMACS software and the CHARMM force field. Simulations were performed under normal temperature and pressure conditions to explore the system's structure and dynamic behaviour, providing a foundation for further understanding and optimizing the system's performance. The entire simulation system, including POPG lipid, drug molecules (LTX-315), sodium ions, and water molecules, was constructed using PACKMOL. The initial simulation box size was set to 8 nm × 8 nm × 8 nm. The CHARMM36 force field was used to describe interactions within the POPG lipid, while the CHARMM General Force Field was employed for LTX-315. Appropriate force field parameters were assigned to each atom and bond type based on the chemical structures of the components. GROMACS 2018.4 was utilized to perform energy minimization and NPT ensemble simulations on the system. The simulation timestep was set to 2 fs, and the total simulation duration was 100 ns. The temperature was controlled using the V-rescale method, and pressure coupling was applied using the Berendsen algorithm. The NPT ensemble was employed for the molecular dynamics simulation, allowing for the simulation of the trajectories and interactions of the atoms in the system. Molecular electrostatic potential maps were calculated at

the B3LYP-D3(BJ)/6-31G(d)* level of theory by using Gaussian 16 (C.01) [43].

SEM observation

Overnight cultures of *E. coli* 25922 and MRSA 43300 were diluted in fresh LB broth at a dilution factor 1:10,000 and subsequently incubated at 37 °C, 250 rpm for 2 h. Following this incubation, the strains were treated with 2 × MIC of LTX-315 for 1 h in 6-well plates, with untreated groups designated controls. Each well contained a square indium tin oxide (ITO) coated glass slide (Merck, 50926–11-9), which was gently washed with PBS at pH 7.4 and fixed overnight at 4 °C in 4 % Paraformaldehyde Fix Solution (PFM, Santa Cruz Biotechnology, E1622). To dehydrate the samples, they were washed three times with PBS to eliminate paraformaldehyde and then subjected to sequential dehydration using ethanol at 50 %, 70 %, 90 %, and 100 %, with each concentration applied for 15 min. Subsequently, the slides were then coated with a layer of gold and observed using a Scanning Electron Microscope (Tescan, VEGA3).

Cytotoxicity assay

The cytotoxic effects of LTX-315 were evaluated utilizing the Cell Counting Kit-8 (CCK-8, MCE, HY-K0301). The HEK293 (ATCC CRL-1573) and Hep G2 (ATCC HB-8065) cell lines were maintained in Dulbecco's Modified Eagle Medium (DMEM) enriched with 10 % Fetal Bovine Serum. Following a 24-hour incubation period at 37 °C in a 5 % CO_2, the culture medium was substituted with fresh medium containing varying concentrations of LTX-315. The plates were then incubated for 24 h under the same conditions. Subsequently, WST-8 was introduced to each well, and the absorbance at 450 nm was quantified using a CLARIOstar microplate reader after a 2-hour incubation period. Each experiment was biologically replicated three times.

Hemolysis assay

The 8 % sheep blood cells were washed with phosphate-buffered saline (PBS) until the supernatant was transparent. Subsequently, 1 mL of the 8 % blood cell suspension was incubated with serially diluted concentrations of LTX-315, ranging from 0 to 160 μM, for one hour at 37 °C. Triton X-100 at a concentration of 0.2 % and PBS were pointed as positive and negative controls, respectively. Following incubation, the samples were centrifuged at 3,000 × g for 10 min, and 100 μL of the supernatant from each group was transferred to a 96-well plate for absorbance measurement at 450 nm using a microplate reader (CLARIOstar). Each experiment was biologically replicated three times.

Cytochrome P450 assay

The influence of LTX-315 on Cytochrome P450 (CYP450) was assessed using the Vivid CYP450 screening kit [44]. Three CYP450 enzymes (CYP2C9, CYP2C19, and CYP3A4) were used in this assay, supplied by the Vivid CYP2C9 Green (Thermo Scientific, P2860), Vivid CYP2C19 Blue (Thermo Scientific, P2864), and Vivid CYP3A4 Green (Thermo Scientific, P2857) kits. The test compound was prepared by diluting it to a concentration of 2.5 times in a 1X Vivid CYP450 reaction buffer. Known positive inhibitors for specific P450 enzymes were also prepared: sulfaphenazole (CYP2C9 inhibitor), miconazole (CYP2C19 inhibitor), and ketoconazole (CYP3A4 inhibitor), all components were solubilized in 1X Vivid CYP450 reaction buffer.

In a 96-well plate, 40 μL of the prepared samples were blended with the Master Pre-Mix, which consists of CYP450 Baculosomes Plus reagent and the Vivid regeneration system, to achieve a total reaction volume of 50 μL. This mixture was incubated at room temperature for 10 min. The reaction was subsequently initiated by adding 10 μL of a 10X Vivid substrate and $NADP^+$ mixture to each well. Following another 10-minute incubation, the reaction was terminated by adding 0.5 M Tris base stop reagent. Fluorescence measurements were then taken at designated excitation and emission wavelengths: 485 nm and 520 nm for CYP2C9 and CYP3A4 and 415 nm and 460 nm for CYP2C19. The inhibition rate was determined using the formula:

$$\%inhibition = \left(1 - \frac{X - B}{A - B}\right) \times 100\% \quad (3)$$

where X denotes the fluorescence measurement of the test compounds, A signifies the fluorescence measurement recorded in the absence of an inhibitor, and B represents the fluorescence measurement obtained in the presence of a positive control. Each experiment was biologically replicated three times.

Marine infection model

The therapeutic effect of LTX-315 on the clinical strain Hvkp2 (carbapenem-resistant and hypervirulent) reported in our previous studies was evaluated in a mouse infection model [23]. Four to six-week-old female ICR mice were used in this study and randomly assigned to five groups (5 mice per group). All mice were infected with 100 μL of a bacterial suspension (6×10^5c.f.u. per mouse) via intraperitoneal injection to induce infection. One hour post-infection, the mice were administered LTX-315 via intraperitoneal injection at three different dosage levels: low (5 $mg{\cdot}kg^{-1}$), medium (10 $mg{\cdot}kg^{-1}$), and high (20 $mg{\cdot}kg^{-1}$). One group was treated with meropenem with 20 $mg{\cdot}kg^{-1}$. Drugs were administered every 12 h for a total of five doses. Mice survival was monitored for 7 days after infection.

Statistical analysis

The data presented in this study were expressed as means ± standard deviation (SD). The sample size (n) for statistical analysis was three, and the statistical significance between two groups was assessed using the unpaired Student's t-test. The one-way ANOVA was employed for comparing more than two groups. Furthermore, the statistical significance of survival curves was determined using the Log-rank (Mantel-Cox) test. A P-value < 0.05 was considered statistically significant, while P > 0.05 was deemed statistically insignificant (denoted as ns). All statistical analyses were conducted using GraphPad Prism 8.

Results

Antibacterial Activity of LTX-315

The antibacterial activity of LTX-315 was assessed using the broth microdilution method. As shown in Table 1, LTX-315 exhibits a broad bactericidal spectrum, particularly effective against antibiotic-resistant strains such as carbapenem-resistant *E. coli*, polymyxin E-resistant, and methicillin-resistant *Staphylococcus aureus* (MRSA). In contrast to other antibiotics, such as polymyxin E, limited by the bacterial class it targets, and gentamicin, which faces bacterial resistance, LTX-315 demonstrates significant efficacy across a wide range of tested bacterial strains. These results indicate its potential to treat infections caused by multidrug-resistant bacteria.

Table 1
Activity of LTX-315 against microorganisms.

Organism	MIC(μM)				
	LTX-315	PE	GEN	EM	CHX
S. aureus 29213	7.5	>91.38	2.6	0.34	0.8
S. aureus 1717	7.5	>91.38	1.3	87	1.6
S. aureus 43300(MRSA)	3.75	91.38	>166	>174	3.2
S. aureus 1174 (MRSA)	7.5	>91.38	5.2	0.34	1.6
S. aureus 86 (MRSA)	7.5	>91.38	2.6	>174	1.6
S. aureus 86I (MRSA)	7.5	>91.38	>166	>174	1.6
S. aureus 88 (MRSA)	7.5	>91.38	>166	0.34	3.2
S. aureus 11I4 (MRSA)	7.5	>91.38	83	>174	1.6
B. cereus 177	3.75	>91.38	>166	0.17	3.2
B. cereus 107 (CR)	1.875	>91.38	>166	0.68	3.2
Vibrio 1978	3.75	1.43	5.2	10.9	25.5
Vibrio 1853 (PER)	3.75	2.86	5.2	>174	3.2
E. coli 25922	7.5	1.43	2.6	87	6.4
E. coli 5 (PER)	7.5	5.72	>166	>174	25.6
E. coli CL-4 (CRE)	7.5	2.86	>166	>174	12.8
E. coli BJE-4 (CRE)	7.5	1.43	>166	>174	6.4
E. coli (MCR-1)	7.5	5.72	2.6	174	3.2
E. coli (NDM-1)	15	1.43	1.3	43.5	6.4
K. pneumoniae MGH78578	120	2.86	166	174	102
K. pneumoniae 2 (CRE and 3GCRE)	7.5	91.38	>166	>174	51
K. Pneumoniae HKU57 (CRE and TGCR)	3.75	2.86	>166	>174	12.8
K. Pneumoniae FJ-8 (CRE)	30	11.42	>166	>174	102
P. aeruginosa 18C53 (CR)	30	2.86	5.2	>174	51
P. aeruginosa 18C54 (CR)	30	2.86	>166	>174	102
A. baumannii 17,978	30	2.86	2.5	43.5	25.6
A. baumannii R44(CR and PER)	1.875	45.7	10.4	>174	>204
A. baumannii R550(CR)	15	45.7	>166	21.8	12.8

PE: polymyxin E; GEN: Gentamycin; EM: Erythromycin; CHX: Chlorhexidine Diacetate; CR: carbapenem-resistant; PER: polymyxin E resistant; CRE: carbapenem-resistant Enterobacterales; 3GCRE: third-generation cephalosporin-resistant Enterobacterales; TGCR: Tigecycline resistant; *B. cereus*: *Bacillus cereus*; *A. baumannii*: *Acinetobacter baumanni*; *P. aeruginosa*: *Pseudomonas aeruginosa*.

To investigate the potential bactericidal mechanism of LTX-315, we considered its oncolytic properties and molecular weight, employing a strategy that examines interactions from the outside of the cell inward. We selected *E. coli* 25922 (gram-negative) and *S. aureus* 43300 (gram-positive) as representative strains for this study. The influence of lipopolysaccharides (LPS), the outermost layer of gram-negative bacteria, was evaluated; no significant increase in the minimum inhibitory concentration (MIC) was observed even at a high LPS concentration of 256 μg/mL (Fig. 1**A**). A similar trend was noted for MRSA 43300, where bactericidal effects were inhibited at much higher lipid-to-LTX-315 ratios (**Fig. S1A**). Two phospholipids, 1-palmitoyl-2-oleoyl-*sn*-glycero-3-phosphoethanolamine (POPE) and 1-palmitoyl-2-oleoyl-*sn*-glycero-3-phospho-(1′-*rac*-glycerol) (POPG), which are key components of the inner leaflet of the outer membrane, were also examined. POPG was found to antagonize the effects of LTX-315 at a low concentration of 32 μg/mL, whereas POPE required a higher concentration of 128 μg/mL to exhibit similar effects for *E. coli* 25922 (Fig. 1**B,** Fig. 1**C**). Besides, POPG with 32 μg/mL ceases LTX-315 to be effective, while POPE does not influence its bactericidal effect for MRSA 43300 (**Fig. S1B** and **Fig. S1C**). Furthermore, colistin, another peptide antibiotic, demonstrated reduced efficacy in the presence of POPG at a lower concentration of 16 μg/mL (**Fig. S1D**).

To evaluate whether increased outer membrane permeability could enhance LTX-315′s bactericidal effect, we combined it with polymyxin B nonapeptide (PMBN), an outer membrane permeabilizer [45]. However, results indicated no significant correlation between outer membrane permeability and bactericidal efficacy (**Fig. S1E and S1F**). The results suggest that LTX-315 primarily interacts with membrane components, particularly POPG. Time-killing curves for LTX-315 in the presence of exogenous POPG or POPE were generated to verify this hypothesis further. In stark contrast to the control (2 × MIC), both concentrations of POPG (32 and 128 μg/mL) completely negated the bactericidal effect against *E. coli* 25922 (Fig. 1**D**). A similar phenomenon was observed for MRSA 43300 (**Fig. S2A**). Conversely, POPE only weakened the bactericidal effect at high concentrations (128 μg/mL), but no surviving cells were detected (Fig. 1**E**). For MRSA 43300, survival depended on POPE concentration, with significantly fewer cells than the untreated group (**Fig. S2B**). Additionally, LTX-315 displayed a strong destructive effect on liposomes composed of phospholipids (Fig. 1**I**). These findings indicate that LTX-315 likely exerts its bactericidal effects primarily through interactions with POPG. Given the net negative charge of POPG (**Fig. S3B**) and the positive charge of LTX-315, we hypothesized a strong electrostatic interaction between the two.

The MIC of LTX-315 under varying pH conditions or with the addition of cations was also evaluated. Results showed that MIC increased with acidity and decreased with alkalinity (Fig. 1**G, S2C**). At low pH, the head of phosphatidylglycerol (PG) becomes protonated, causing a conformational change from a perpendicular to a parallel orientation relative to the membrane. In contrast, the headgroup maintains a perpendicular orientation at neutral or alkaline pH, as described by Sanson et al [46]. Protonation and conformational transition would weaken LTX-315′s binding to PG, thus reducing its bactericidal effect. Fe^{3+} had the most pronounced impact among the tested cations, followed by Fe^{2+} (Fig. 1**H, S2D**). Typically, cations occupy spaces between negatively charged phosphate groups, potentially neutralizing the net charge. Sufficient ionic strength can also induce a similar conformational change in the headgroup [47]. Divalent cations like Mg^{2+} and Ca^{2+} can diminish the effectiveness of cationic antimicrobial peptides against gram-negative bacteria [48].

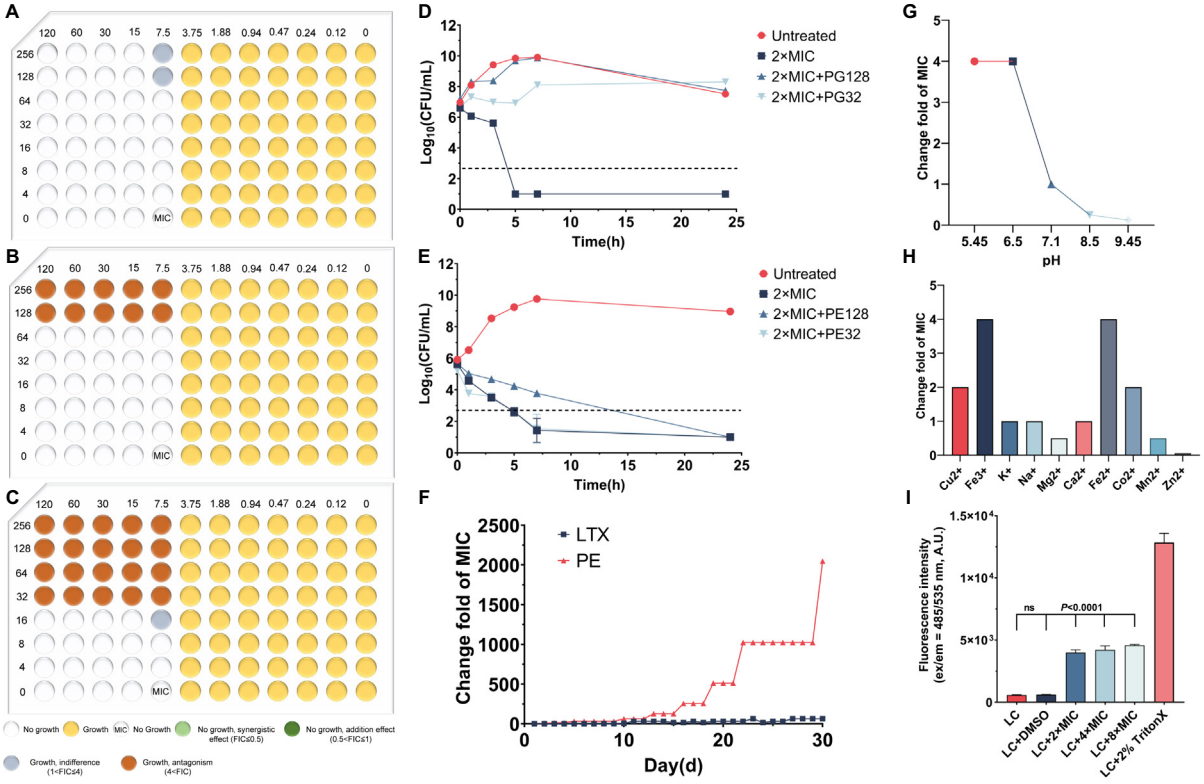

Fig. 1. Bactericidal ability and resistance determination of LTX-315 *in vitro*. (A) The influence of lipopolysaccharide (LPS) on the bactericidal effect of LTX-315 on *E. coli* 25922 (n = 3). (B) The influence of 1-palmitoyl-2-oleoyl-*sn*-glycero-3-phosphoethanolamine (POPE) on the bactericidal effect of LTX-315 on *E. coli* 25922 (n = 3). (C) The influence of 1-palmitoyl-2-oleoyl-*sn*-glycero-3-phospho-(1′-*rac*-glycerol) (POPG) on the bactericidal effect of LTX-315 on *E. coli* 25922 (n = 3). (D) The time-killing curve of LTX-315 (2 × MIC) on *E. coli* 25922 and under treatment with PG. Data are indicative of three independent experiments ± standard deviation. (E) The time-killing curve of LTX-315 (2 × MIC) on *E. coli* 25922 and under treatment with PE. Data are indicative of three independent experiments ± standard deviation. (F) Induced-resistance assay of *E. coli* 25922 to LTX-315 (LTX) and polymyxin E (PE) within 30 days. (G) The change in minimum inhibitory concentrations (MIC) of LTX-315 for *E. coli* 25922 under various pH conditions. Data are indicative of three independent experiments ± standard deviation. (H) The change in MIC of LTX-315 for *E. coli* 25922 under various exogenous additions of cations. Data are indicative of three independent experiments ± standard deviation. (I) The damage caused by LTX-315 at different concentrations (2 × MIC, 4 × MIC, 8 × MIC) to Liposome-Calcein (LC). The dashed line in (D) and (E) represents the detection lower limit. Data are indicative of three independent experiments ± standard deviation. The nonparametric one-way ANOVA was applied to calculate statistical significance for (I); $P < 0.05$ was considered significant, while ns was insignificant.

Consequently, these cations could neutralize the net negative charge of POPG, weakening its electrostatic interaction with LTX-315 and diminishing its bactericidal effects. Overall, we propose that the bactericidal mechanism of LTX-315 involves interaction with the membrane component PG, leading to membrane damage. This mechanism may also reduce the likelihood of bacterial resistance compared to colistin (Fig. 1**F**). RNA sequencing results related to LTX-315 are presented in **Fig. S10**.

Mode of interaction between LTX-315 and POPG

To further elucidate the interaction between LTX-315 and PG, nuclear magnetic resonance (NMR) spectroscopy was employed. The structure of LTX-315 is depicted in Fig. 2**A**, highlighting the regions with indole groups in pink circles. The NMR spectrum of LTX-315, along with its proton assignments, is shown in **Figs. S4-S5A, B, and C** through ^{1}H–^{1}H COSY, ^{1}H–^{1}H NOESY, and ^{1}H–^{13}C HSQC spectra. For a detailed assessment of the interactions, we acquired ^{1}H NMR spectra of LTX-315 in the presence of PG with varying charged head groups in D_2O. As illustrated in Fig. 2**B**, the proton signals of LTX-315 significantly diminished upon the addition of negatively charged PG, nearly vanishing with 2 M equivalents, indicating a strong interaction. Concurrently, the proton signals from the tryptophan moieties shifted towards higher field regions, suggesting that LTX-315 becomes entrapped within PG micelles, with the indole group likely preferentially interacting with PG. In contrast, NMR spectra obtained with extra addition neutral phospholipid PE showed no loss of resonance signal, even at three times the molar amount of LTX-315 (**Fig. S3A and S5D**). These results indicate that LTX-315 has a strong affinity for negatively charged phospholipids, particularly at the indole moieties. The high affinity of LTX-315 for PG was also validated via Isothermal Titration Calorimetry (ITC), demonstrating a K_d value in the nanomolar range at 0.044 ± 0.022 μM (Fig. 2**C**). Due to the strong interaction with PG, almost no proton signals were detected in the main chain region of the one-dimensional hydrogen spectra, likely due to long T1 relaxation times and very short T2 relaxation times, preventing the observation of other potential binding areas.

We conducted an electrostatic potential (ESP) distribution analysis of the LTX-315 surface to support our findings further. As shown in Fig. 2**D**, among the three most positive ESP regions, the most significant was identified as region 10, followed by the other two locations of the indole groups. All positive ESP regions likely contribute to the electrostatic interaction. Additionally, molecular dynamics simulations indicated a stable complex structure formation between LTX-315 and PG, with results presented in Fig. 2**E** for simulations at 100 ns. Details can be referred to the **Fig. S6A-D**. Besides the previously mentioned aromatic amines, we also observed strong interactions with fatty amines from the dynamics. These data indicate a robust interaction between LTX-315 and PG, highlighting potential binding sites.

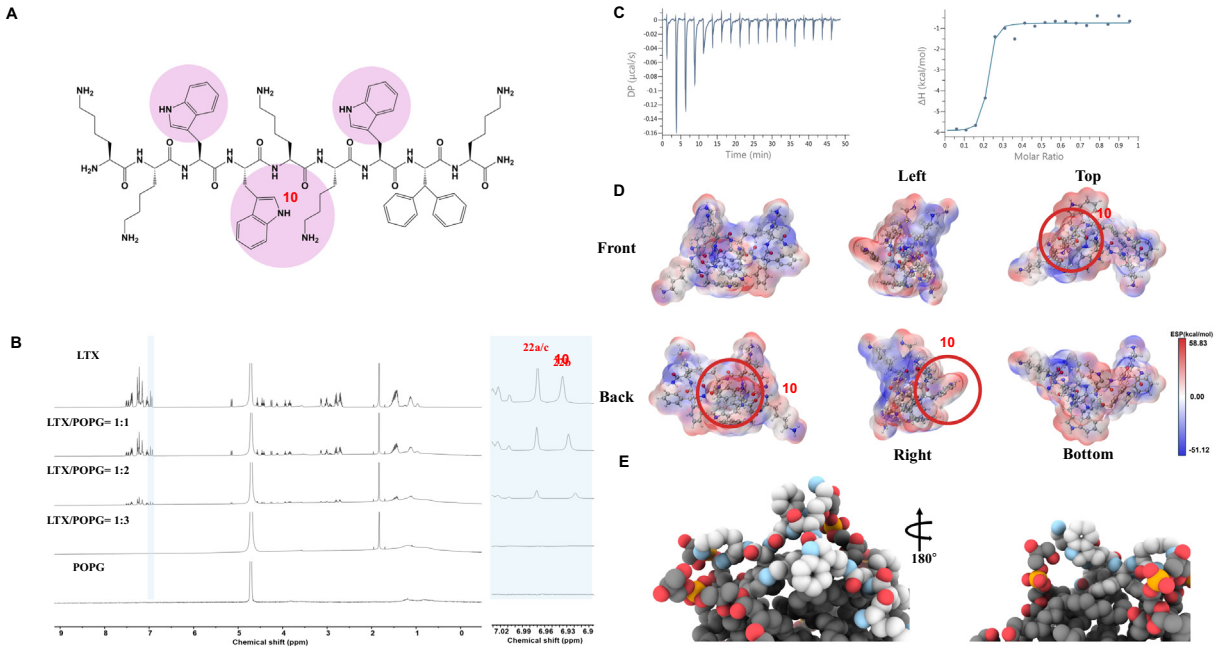

Fig. 2. The interaction of LTX-315 with POPG. (A) The chemical structure of LTX-315. The pink region represents the positive charge characteristic in the electrostatic potential. (B) ^{1}H NMR spectra of LTX-315 (acetate) with different molar equivalents of POPG. (C) The isothermal titration calorimetry result of LTX-315 with PG. (D) Electrostatic potential distribution of LTX-315 at various angles. The single arrow indicates the spin direction, while the double arrows indicate the spin down first. The blue parts represent negative potential energy, and the red represents positive potential energy. The unit of ESP is kcal/mol. (E) The structure of the LTX-315-POPG complex at 100 ns from different angles. (For interpretation of the references to colour in this figure legend, the reader is referred to the web version of this article.)

Impact of LTX-315 on bacterial membrane properties

Despite our understanding of LTX-315′s interaction with POPG, the bactericidal mechanism remains unclear. To address this, we conducted assays to investigate the impact of LTX-315 on the bacterial membrane following its combination with POPG. The permeability of the outer membrane increased when treated with LTX-315 at 1/2 × MIC (Fig. 3**A**). The result suggests that NPN could diffuse significantly into the hydrophobic region of the membrane after LTX-315 interacts with POPG, resulting in an increased fluorescence signal [33]. Additionally, LTX-315 substantially impacted membrane integrity, observable both at endpoint measurements and during dynamic assessments. Notably, even at low concentrations (1/2 × MIC), LTX-315 caused rapid membrane damage (Fig. 3**B, 3D**). MRSA 43300 exhibited a more pronounced response than *E. coli* 25922, as shown in **Figs. S7A and S7C**. This difference may be attributed to the primary membrane components: PG in *S. aureus* versus PE in *E. coli* [49,50]. The interaction between LTX-315 and PG may alter the structure and dynamics of the membrane, leading to an energetically unfavourable configuration that compromises membrane integrity.

We also examined membrane fluidity, which became more rigid following the LTX-315 treatment (Fig. 3**C**). The binding of metal cations to the phospholipid headgroup increases the average molecular weight of phospholipids, thus impeding lateral lipid diffusion [47]. The interaction between LTX-315 and POPG likely causes the latter to become fixed, reducing membrane fluidity. This was further confirmed in MRSA 43300, where a significant reduction in fluidity was also observed (**Fig. S7B**). Next, we assessed the membrane potential of the bacteria, finding that LTX-315 (1/2 × MIC) significantly affected the potential difference across the membrane (Fig. 3**E**). Over time, environmental DNA, RNA, and protein levels increased, dependent on LTX-315 concentration compared to untreated controls (Fig. 3**F, 3G, 3H**). To further confirm membrane damage, we employed the ONPG assay, which revealed that colourless ONPG was hydrolyzed by β-galactosidase to produce yellow-on-G, indicating extracellular enzyme activity and, thus membrane damage (Figs. 3**I, S7D**). Microscopic observations confirmed the destructive impact of LTX-315 on cell membranes, showing that cells fragmented into smaller pieces, with some wholly disintegrated (Fig. 3**J, 3 K**). The cell membrane's breakdown and intracellular contents' release were also visually confirmed (**Figs. S7E, S7F**). In summary, LTX-315 damages the bacterial cell membrane, altering its properties and contributing to its bactericidal effect. The action mode of LTX-315 is shown in Fig. 4 **(A-F)**.

Effect of LTX315 on intracellular biochemical index

Following our findings on the membrane effects of LTX-315, we investigated physiological changes within the cells. Damage to lipids, DNA, and proteins typically elevates intracellular levels of reactive oxygen species (ROS) [51]. Fig. 5**A and S8A** show that total ROS levels in *E. coli* 25922 and MRSA 43300 increased significantly with LTX-315 treatment (1/2 × MIC, 1/4 × MIC, 1/8 × MIC). Further analyses were conducted to identify specific types of ROS. Fig. 5**B and 5D** indicate that NO and $^{-}$OCl levels significantly increased, while hydroxyl radicals (•OH) showed no notable change (Fig. 5**E**). In MRSA 43300, •OH levels declined over time, although NO and $^{-}$OCl−OCl exhibited similar increases as in *E. coli* (**Figs. S8B, S8E, S8F**). Additionally, H_2O_2 levels rose significantly, depending on the concentration of LTX-315 (Fig. 5**H, S8I**). This high production of ROS may disrupt the intracellular redox state.

Subsequently, we measured peroxidase activity to assess ROS scavenging capacity [52]. Fig. 5**I and S8J** support our hypothesis, showing a decreased ability to neutralize ROS. ATP levels were also evaluated for bacterial survival and cellular processes. Both intracellular and extracellular ATP levels dramatically reduced in response to LTX-315, with extracellular ATP levels rising concurrently (Fig. 5**G, S8K**). We also measured NAD^{+} and NADH levels,

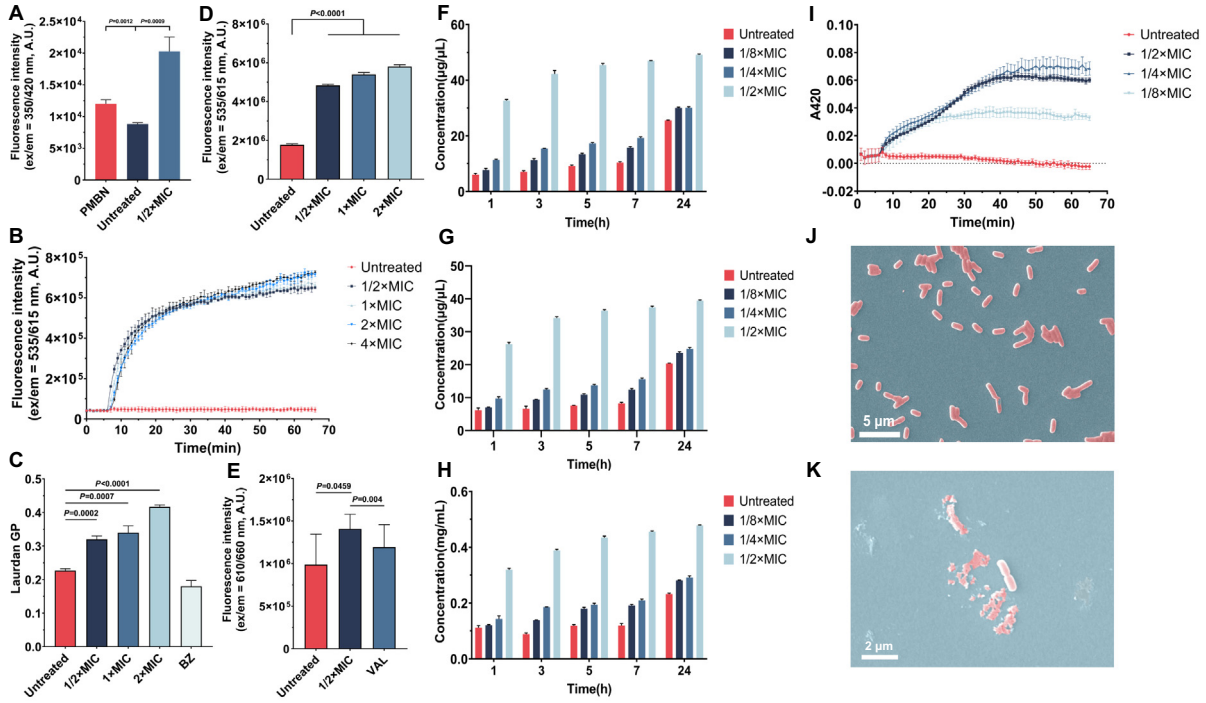

Fig. 3. The influence of LTX-315 on the *E. coli* 25922 membrane (A) The outer membrane permeability of *E. coli* 25922 under treatment with LTX-315 (1/2 × MIC). (B) Dynamic determination of membrane integrity in *E. coli* 25922 under various LTX-315 concentrations (1/2 × MIC, 1 × MIC, 2 × MIC, 4 × MIC). (C) Determination of membrane fluidity in *E. coli* 25922 treated with LTX-315 at 1/2 × MIC, 1 × MIC, 2 × MIC. BZ denotes 30 mM benzyl alcohol. (D) Endpoint determination of membrane integrity in *E. coli* 25922 under LTX-315 treatment at 1/2 × MIC, 1 × MIC, 2 × MIC. (E) Determination of membrane potential in *E. coli* 25922 under 1/2 × MIC LTX-315 treatment. VAL indicates 5 mg/ml valinomycin. (F) DNA leakage determination in *E. coli* 25922 treated with LTX-315 at 1/2 × MIC, 1/4 × MIC, 1/8 × MIC. (G) RNA leakage determination in *E. coli* 25922 treated with LTX-315 at 1/2 × MIC, 1/4 × MIC, 1/8 × MIC. (H) Protein leakage determination in *E. coli* 25922 treated with LTX-315 at 1/2 × MIC, 1/4 × MIC, 1/8 × MIC. (I) β-galactosidase activity determination in *E. coli* 25922 treated with LTX-315 at 1/2 × MIC, 1/4 × MIC, 1/8 × MIC. The substrate used is *ortho*-Nitrophenyl-β-galactoside (ONPG). (J) Scanning electron microscopy of untreated *E. coli* 25922. (K) Scanning electron microscopy of *E. coli* 25922 treated with 2 × MIC LTX-315. Data are representative of 3 independent experiments ± standard deviation. The unpaired student's *t*-test calculated statistical significance for (A), (C), and (E), while the nonparametric one-way ANOVA calculated statistical significance for (D); $P < 0.05$ was considered significant, while ns was insignificant.

key players in energy metabolism [53]. LTX-315 treatment resulted in notable decreases in NAD^+ and NADH, with NADH depletion being more pronounced, thus significantly increasing the NAD^+/NADH ratio (Fig. 5**C, 5F, S8C**). Interestingly, MRSA 43300 exhibited an opposite trend, with increased NAD^+ and NADH levels leading to an elevated NAD^+/NADH ratio (**Figs. S8D, S8G, S8H**). The NAD^+/NADH ratio imbalance may hinder ATP synthesis [54]. LTX-315′s impact on membrane properties, such as proton motive force, could also affect ATP production [55]. In summary, LTX-315 increases intracellular ROS levels (especially NO, ^-OCl, and H_2O_2) while inhibiting peroxidase activity. It also depletes ATP production by affecting the NAD^+/NADH redox ratio, enhancing its bactericidal effect.

Safety and in vivo efficacy of LTX315 as an antibiotic

The safety of LTX-315 is crucial for its potential clinical application. We assessed LTX-315′s safety through several assays. A low resistance frequency (calculated at $< 10^{-9}$) was observed, with no colonies growing after incubation at 37 °C for 48 h. Next, we evaluated the impact of LTX-315 on the viability of HEK293 and HepG2 cells. No significant decrease in cell viability was noted (Fig. 6**A, B**), indicating low toxicity to these cell lines. Given that mammalian cells primarily contain phosphatidylcholine (PC), while LTX-315 targets PG, we examined the influence of PC on LTX-315′s bactericidal effect. As expected, the addition of PC did not affect the MIC of LTX-315 (**Figs. S9A, S9B**), explaining the maintained viability in the above-tested cell lines. We also assessed hemolytic activity, another critical safety indicator. Fig. 6**D** shows LTX-315 exhibits extremely low hemolytic activity, even at high concentrations (160 μM). However, LTX-315 did demonstrate varying inhibitory effects on CYP450 enzymes (Fig. 6**C, 6E, 6F**), potentially impacting drug metabolism. Finally, we tested the in vivo efficacy of LTX-315. Fig. 6**G** indicates a favourable treatment effect, with LTX-315 significantly improving survival rates in mice infected with hypervirulent *K. pneumoniae*.

Discussion

The phenomenon of antimicrobial resistance is increasingly severe on a global scale, presenting a significant public health challenge that transcends national borders and social classes. The emergence of multi-resistant bacterial strains poses formidable obstacles to effective clinical treatment. This reality underscores the need to discover, develop, and synthesize novel antibacterial compounds. Encouragingly, efforts from research institutions worldwide have yielded promising results. For instance, teixobactin, a depsi-peptide isolated from uncultured soil bacteria, showcases a potent bactericidal effect against *Staphylococcus aureus* and *Mycobacterium tuberculosis*, with a low incidence of resistance [29]. Similarly, clovibactin, another compound derived from soil bacteria, effectively combats drug-resistant strains, particularly gram-negative bacteria, without observable resistance [56]. Furthermore, Zampaloni et al. introduced a novel class of compounds tailored to target carbapenem-resistant *Acinetobacter baumannii* [57], while the short linear peptide SLAP-S25 augments the effectiveness of established antibiotics like colistin and vancomycin, despite exhibiting minimal antibacterial activity itself [58]. These

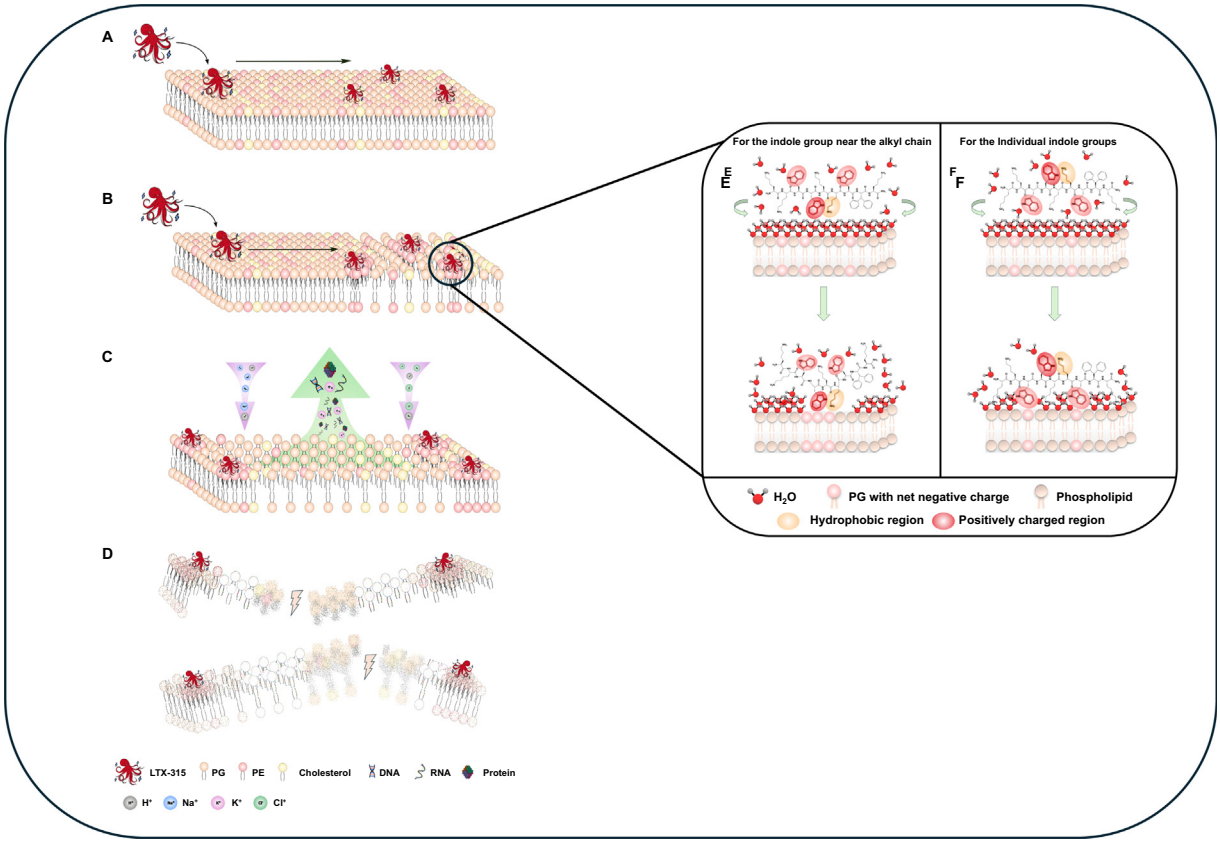

Fig. 4. The action mode of LTX-315. (A) The LTX-315 contacts with the membrane of bacteria. (B) The LTX-315 interacts with multiple negatively charged PGs through its multiple positively charged regions and limits the movement of PGs. (C) The remaining phospholipid molecules will rearrange due to fluidity, but the gaps between them will increase, resulting in increased permeability. Materials such as DNA, RNA, and protons move in and out of cells more easily by adapting to the concentration gradient. (D) At a certain membrane surface area, the strength of the cell membrane and its mechanical support will be significantly weakened as more LTX-315 molecules interact with PG, ultimately leading to rupture once a critical threshold is reached. (E) The recognize and binding process between the indole group near the alkyl chain (LTX-315) and the PG. (F) The recognize and binding process between the individual indole groups (LTX-315) and the PG.

findings are encouraging, yet the antimicrobial spectrum of these compounds remains limited, highlighting the need for broader-spectrum agents suitable for various infections.

In this study, LTX-315 exhibited a relatively broad spectrum of activity, demonstrating significant bactericidal effects against gram-positive and gram-negative bacteria, including multi-resistant pathogens. Notably, LTX-315 improved survival rates in mice infected with hypervirulent *Klebsiella pneumoniae* resistant to carbapenems, often considered last-resort treatments. This efficacy suggests that LTX-315 could have broader applications in combating bacterial infections. Furthermore, its low resistance frequency positions LTX-315 as a promising candidate for clinical trials, particularly in contrast to colistin, which is effective but frequently leads to resistance [59].

Our analysis of LTX-315′s interactions with phospholipid components, particularly PG, revealed insights into its mechanism of action. By examining NMR spectra, we identified significant interactions between the indole group and the alkyl chain of LTX-315 with the negatively charged phosphate groups of PG. The hydrophobic microenvironment created by the alkyl chain may enhance the recognition of phosphate anions in aqueous solutions, establishing a preferential binding site that increases efficacy [60]. Given the increasing interest in antibacterial peptides, these findings may guide the synthesis of novel peptides with stronger interactions with PG, potentially improving their effectiveness.

Importantly, PG constitutes approximately 20–25 % of the membrane in *E. coli* and about 55 % in *S. aureus*, while it is found in only about 2 % of mammalian cell membranes [61,62]. This disparity suggests that LTX-315 exerts its bactericidal effects through a mechanism that minimally impacts mammalian cells, thus ensuring selectivity and safety. Additionally, PG presents a viable target for developing new antibacterial compounds. Advanced methods such as solid-phase peptide synthesis or microwave-assisted synthesis could greatly expedite the production of these peptides, facilitating industrial-scale manufacturing [63,64].

AMPs demonstrate broad-spectrum or specific bactericidal activity depending on their specific targets. For example, vancomycin effectively eliminates Gram-positive bacteria by binding to the D-Ala-D-Ala peptide motif of the peptidoglycan precursor, thereby inhibiting cell wall synthesis. Conversely, colistin targets Gram-negative bacteria by displacing magnesium and calcium ions in the lipopolysaccharide of the outer membrane. Among the commercially available peptide-based antibiotics, only gramicidin D shows activity against Gram-positive and some Gram-negative strains [16]. LTX-315, due to the presence of PG in both Gram-positive and Gram-negative bacteria, demonstrates broad-spectrum activity. Additionally, PG exists on the membrane, making it effective against current multidrug-resistant bacteria.

Concerning safety, the non-specificity of AMPs can lead to cytotoxicity, presenting a significant challenge in clinical treatments [65]. Nephrotoxicity and neurotoxicity are notable and frequent adverse effects that limit the use of polymyxins [66]. The absence of PG in mammalian cells grants LTX-315 a certain degree of safety. Additionally, LTX-315 has demonstrated promising safety performance in a phase II clinical trial for metastatic soft tissue sarcoma [67].

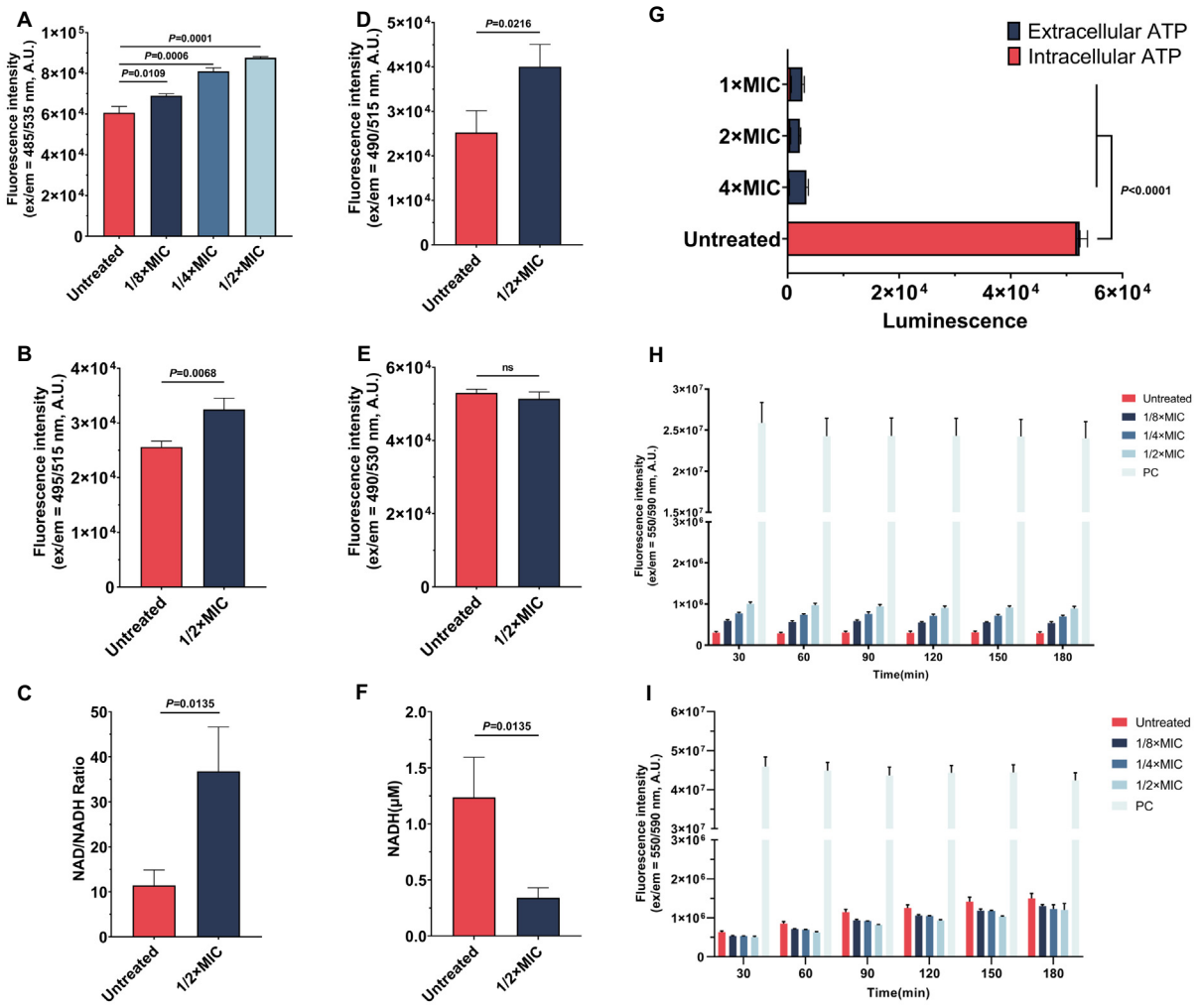

Fig. 5. Determination of the internal physiological indexes of *E. coli* 25922 under treatment with LTX-315. (A) Total reactive oxygen species (ROS) in *E. coli* 25922 under treatment with LTX-315 (1/2 × MIC, 1/4 × MIC, 1/8 × MIC). Data are indicative of three independent experiments ± standard deviation. (B) −OCl content in *E. coli* 25922 treated with LTX-315 at 1/2 × MIC. Data are indicative of three independent experiments ± standard deviation. (C) NAD/NADH ratio in MRSA 43300 treated with LTX-315 at 1/2 × MIC. Data are indicative of three independent experiments ± standard deviation. (D) Nitric oxide (NO) content in *E. coli* 25922 treated with LTX-315 at 1/2 × MIC. Data are indicative of three independent experiments ± standard deviation. (E) Hydroxyl radical (OH) content in *E. coli* 25922 treated with LTX-315 at 1/2 × MIC. Data are indicative of three independent experiments ± standard deviation. (F) NADH content in *E. coli* 25922 treated with LTX-315 at 1/2 × MIC. Data are indicative of three independent experiments ± standard deviation. (G) ATP content in *E. coli* 25922 treated with LTX-315 at 1 × MIC, 2 × MIC, 4 × MIC. Data are indicative of three independent experiments ± standard deviation. (H) Hydrogen peroxide (H_2O_2) content in *E. coli* 25922 treated with LTX-315 at 1/2 × MIC, 1/4 × MIC, and 1/8 × MIC over time. Data are indicative of three independent experiments ± standard deviation. (I) Effect of LTX-315 (1/2 × MIC, 1/4 × MIC, 1/8 × MIC) on the peroxidase activity in *E. coli* 25922. Error bars indicate the standard deviation for the plots mentioned above. Data are indicative of three independent experiments ± standard deviation. The unpaired student's *t*-test calculated statistical significance for (A), (B), (C), (D), (E), and (F), while the nonparametric one-way ANOVA was calculated statistical significance (G); $P < 0.05$ was considered significant, while ns was insignificant.

As stated in the introduction, bacteria may deactivate antibiotics through enzymatic hydrolysis or by altering the binding site via gene mutation. Consequently, peptides targeting intracellular components like ribosomes may be more prone to causing drug resistance. In contrast, LTX-315 inflicts rapid physical damage to bacterial membranes by strongly binding to PG, reducing the likelihood of resistance development [68]. Overall, these advantages of LTX-315 contribute to overcoming the challenges faced by AMPs.

Inspired by LTX-315, a novel strong binding mechanism with PG enhances the ability to recognize anions in aqueous environments, which could catalyze the design of pharmacotherapeutic agents with improved efficacy. Optimizing the recognition of phosphate anions may strengthen electrostatic interactions with bacterial membranes, offering a pathway to enhanced drug performance. For instance, a series of 1,4,7-triazacyclononan macrocycles linked by rigid aromatic motifs compounds can bind phosphate anions in acidic circumstances [69]. In addition, a P-loop-type nest contained in a hexapeptide can strongly bind with dihydrogen phosphate ions in water at neutral pH [70]. The anion-recognition moiety of $C^{a}NN$ consists of two main-chain amide hydrogen bonds and a C–H hydrogen bond from the next a-carbon atom, which can also bind with the phosphate group [71]. Consequently, future research focuses on how the modification could create hydrophobic, solvent-separated binding domains on peptides that target the membrane, enhancing their recognition and binding ability with PG and deepening our understanding. Moreover, factors like bioavailability and stability are essential and require thorough evaluation.

In addition, due to bacteria's rapid evolutionary adaptations, there is a risk that they may develop resistance to the bactericidal mechanisms we have described. This could occur through redistribution of lipid components, alterations in membrane charge prop-

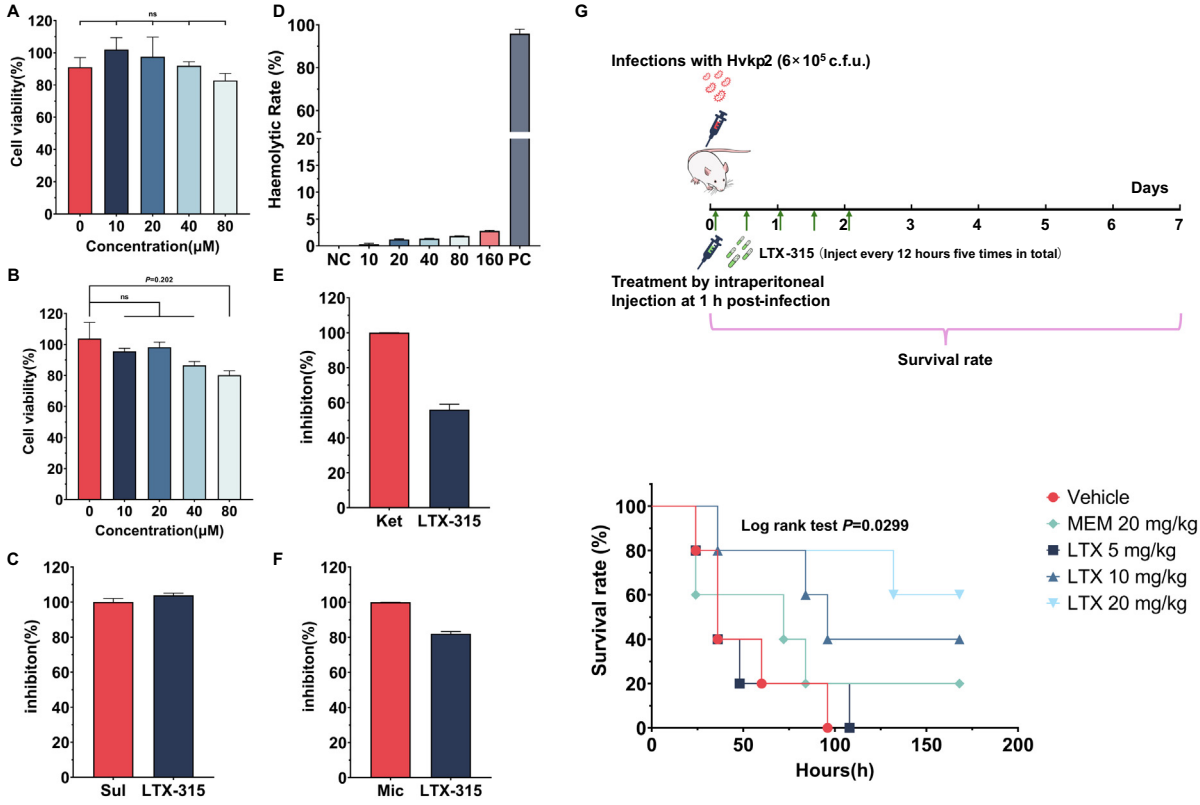

Fig. 6. Determination of the safety and treatment effect of LTX-315. (A) Cell viability of HEK 293 cells treated with LTX-315 (10, 20, 40, 80 μM). Data are representative 3 independent experiments ± standard deviation. (B) Cell viability of HepG2 cells treated with LTX-315 (10, 20, 40, 80 μM). Data are representative 3 independent experiments ± standard deviation. (C) Inhibition effect of LTX-315 on CYP2C9. "Sul" denotes sulfaphenazole (30 μM), a known CYP2C9 inhibitor. LTX-315 concentration was set to 30 μM. Data are representative 3 independent experiments ± standard deviation. (D) Cell viability of HepG2 cells treated with LTX-315 (10, 20, 40, 80 μM). Data are representative 3 independent experiments ± standard deviation. (E) Inhibition effect of LTX-315 on CYP3A4. "Ket" denotes ketoconazole (10 μM), a known CYP3A4 inhibitor. LTX-315 concentration was set to 10 μM. Data are indicative of three independent experiments ± standard deviation. (F) Inhibition effect of LTX-315 on CYP2C19. "Mic" denotes miconazole (30 μM), a known CYP2C19 inhibitor. LTX-315 concentration was set to 30 μM. Data are indicative of three independent experiments ± standard deviation. (G) Survival plot of a mouse model infected with Hvkp2. After infection for one hour, low dose (5 mg/kg, deep blue line), medium dose (10 mg/kg, blue line), and high dose (20 mg/kg, light blue line) of LTX-315 were administered every 12 h for a total of 5 doses. The meropenem (MEM) with 20 mg/kg was antibiotic control. (n = 5 mice per group). The observation period of the survival status was 7 days. The unpaired student's t-test calculated statistical significance for (A) and (B). The Log-rank (Mantel-Cox) test was applied to calculate the significance of the survival curve. $P < 0.05$ was considered significant, while ns was insignificant. (For interpretation of the references to colour in this figure legend, the reader is referred to the web version of this article.)

erties, or de novo biosynthesis of specific functional proteins. Such factors must be considered as we discover and synthesize new compounds targeting bacterial membrane components. Although this work represents a small step forward, our findings could significantly contribute to developing novel antibacterial agents capable of combating multi-resistant bacteria.

Conclusion

In summary, the phenotype assay screening revealed the discovery of LTX-315, a potent bactericidal peptide capable of effectively targeting and eliminating Gram-positive and Gram-negative bacteria, including multidrug-resistant strains. The primary mechanism involves a high-affinity interaction with the membrane component phosphatidylglycerol (PG) at the nanomolar level. Within this process, the specific region housing the indole group and alkyl chain emerges as the key binding site, playing a pivotal role in the peptide's bactericidal activity. The demonstrated efficacy of LTX-315 in both in vitro and in vivo settings validates the success of drug repurposing strategies. It paves the way for developing more potent bactericidal peptides based on anion recognition in water. Future investigations will concentrate on refining the pharmacokinetic properties of LTX-315, assessing its effectiveness in supplementary in vivo models, and investigating combination therapies to bolster its antimicrobial efficacy.

Ethics approval statement

All animal experiments were approved by the Animal Subjects Ethics Sub-Committee of The City University of Hong Kong, and the project number is 8790002RIF.

Funding

This study was supported by the Basic Research Fund of Shenzhen JCYJ20200109143220716, Theme Based Research Scheme (T11-104/22-R), and the Research Impact Fund (R5011-18F) from the Research Grant Council of the Government of Hong Kong SAR.

Declaration of competing interest

The authors declare that they have no known competing financial interests or personal relationships that could have appeared to influence the work reported in this paper.

Acknowledgments

This work was funded by the Basic Research Fund of Shenzhen (grant numbers: JCYJ20200109143220716). This project has received funding from Theme Based Research Scheme (grant numbers: T11-104/22-R). Funding was also provided by the Research Grant Council of the Government of Hong Kong SAR. We extend our gratitude to Liu Shunhe of The Hong Kong University for their valuable assistance in chemical analysis.

Appendix A. Supplementary data

Supplementary data to this article can be found online at https://doi.org/10.1016/j.jare.2024.12.044.

References

[1] Coico R. Gram staining. Curr Protoc Microbiol. 2005;Appendix 3:Appendix 3C.
[2] Zapasnik A, Sokolowska B, Bryla M. Role of lactic acid bacteria in food preservation and safety. Foods 2022;11.
[3] Mackow NA, van Duin D. Reviewing novel treatment options for carbapenem-resistant. Expert Rev Anti-Infe 2024;22:71–85.
[4] Jiang Y, Ding YH, Wei YS, Jian CX, Liu JB, Zeng ZR. Carbapenem-resistant : A challenge in the intensive care unit. Front Microbiol. 2022;13.
[5] Yang XM, Sun QL, Li JP, Jiang Y, Li Y, Lin JP, et al. Molecular epidemiology of carbapenem-resistant hypervirulent in China. Emerg Microbes Infec 2022;11:841–9.
[6] Lee AS, Huttner BD, Catho G, Harbarth S. Methicillin-Resistant *Staphylococcus aureus*: An Update on Prevention and Control in Acute Care Settings. Infect Dis Clin N Am 2021;35:931–52.
[7] Pulingam T, Parumasivam T, Gazzali AM, Sulaimana AM, Chee JY, Lakshmanan M, et al. Antimicrobial resistance: Prevalence, economic burden, mechanisms of resistance and strategies to overcome. Eur J Pharm Sci 2022;170.
[8] Katz L, Baltz RH. Natural product discovery: past, present, and future. J Ind Microbiol Biotechnol 2016;43:155–76.
[9] Urban-Chmiel R, Marek A, Stepien-Pysniak D, Wieczorek K, Dec M, Nowaczek A, et al. Antibiotic Resistance in Bacteria-A Review. Antibiotics (Basel) 2022;11.
[10] Bertagnolio S, Dobreva Z, Centner CM, Olaru ID, Donà D, Burzo S, et al. WHO global research priorities for antimicrobial resistance in human health. Lancet. Microbe 2024;5.
[11] Kocsis B. Hypervirulent *Klebsiella pneumoniae*: An update on epidemiology, detection and antibiotic resistance. Acta Microbiol Imm H 2023;70:278–87.
[12] Compagne N, Da Cruz AV, Mueller RT, Hartkoorn RC, Flipo M, Pos KM. Update on the Discovery of Efflux Pump Inhibitors against Critical Priority Gram-Negative Bacteria. Antibiotics-Basel 2023;12.
[13] Kyriakidis I, Vasileiou E, Pana ZD, Tragiannidis A. *Acinetobacter baumannii* Antibiotic Resistance Mechanisms. Pathogens 2021;10.
[14] Arnold BJ, Huang IT, Hanage WP. Horizontal gene transfer and adaptive evolution in bacteria. Nat Rev Microbiol 2022;20:206–18.
[15] Dheman N, Mahoney N, Cox EM, Farley JJ, Amini T, Lanthier ML. An Analysis of Antibacterial Drug Development Trends in the United States, 1980-2019. Clin Infect Dis 2021;73:E4444–50.
[16] Browne K, Chakraborty S, Chen RX, Willcox MDP, Black DS, Walsh WR, et al. A New Era of Antibiotics: The Clinical Potential of Antimicrobial Peptides. Int J Mol Sci 2020;21.
[17] Nang SC, Azad MAK, Velkov T, Zhou Q, Li J. Rescuing the Last-Line Polymyxins: Achievements and Challenges. Pharmacol Rev 2021;73:679–728.
[18] Vinogradov AA, Suga H. Introduction to Thiopeptides: Biological Activity, Biosynthesis, and Strategies for Functional Reprogramming. Cell Chem Biol 2020;27:1032–51.
[19] Sacco F, Bitossi C, Casciaro B, Loffredo MR, Fabiano G, Torrini L, et al. The Antimicrobial Peptide Esc(1-21) Synergizes with Colistin in Inhibiting the Growth and in Killing Multidrug Resistant *Acinetobacter baumannii* Strains. Antibiotics (Basel) 2022;11.
[20] Mahlapuu M, Hakansson J, Ringstad L, Bjorn C. Antimicrobial Peptides: An Emerging Category of Therapeutic Agents. Front Cell Infect Microbiol 2016;6:194.
[21] Sveinbjornsson B, Camilio KA, Haug BE, Rekdal O. LTX-315: a first-in-class oncolytic peptide that reprograms the tumor microenvironment. Future Med Chem 2017;9:1339–44.
[22] Weinstein MP, Clinical, Laboratory Standards I. Performance standards for antimicrobial susceptibility testing. 31st edition. ed. Wayne, Pennsylvania: Clinical and Laboratory Standards Institute; 2021.
[23] Gu D, Dong N, Zheng Z, Lin D, Huang M, Wang L, et al. A fatal outbreak of ST11 carbapenem-resistant hypervirulent *Klebsiella pneumoniae* in a Chinese hospital: a molecular epidemiological study. Lancet Infect Dis 2018;18:37–46.
[24] Wu Y, Chen S, Li J, Cai C, Wang H, Zhou M, et al. Surveillance of Multidrug-Resistant Bacterial Infections in Non-Adult Patients - Zhejiang Province, China, 2014-2019. China CDC Wkly 2021;3:1005–13.
[25] Chow HY, Po KHL, Jin K, Qiao G, Sun Z, Ma W, et al. Establishing the Structure-Activity Relationship of Daptomycin. ACS Med Chem Lett 2020;11:1442–9.
[26] Yang X, Ye L, Chan EW, Zhang R, Chen S. Characterization of an IncFIB/IncHI1B Plasmid Encoding Efflux Pump TMexCD1-TOprJ1 in a Clinical Tigecycline- and Carbapenem-Resistant *Klebsiella pneumoniae* Strain. Antimicrob Agents Chemother 2021;65.
[27] Zheng Z, Ye L, Chan EW, Chen S. Identification and characterization of a conjugative bla_{VIM-1}-bearing plasmid in *Vibrio alginolyticus* of food origin. J Antimicrob Chemother 2019;74:1842–7.
[28] Song MR, Liu Y, Li TT, Liu XJ, Hao ZH, Ding SY, et al. Plant Natural Flavonoids Against Multidrug Resistant Pathogens. Adv Sci 2021;8.
[29] Ling LL, Schneider T, Peoples AJ, Spoering AL, Engels I, Conlon BP, et al. A new antibiotic kills pathogens without detectable resistance. Nature 2015;517:455–9.
[30] Pogue JM, Ortwine JK, Kaye KS. Clinical considerations for optimal use of the polymyxins: A focus on agent selection and dosing. Clin Microbiol Infect 2017;23:229–33.
[31] LaPage SP, Efstratiou A, Hill LR. The ortho-nitrophenol (ONPG) test and acid from lactose in Gram-negative genera. J Clin Pathol 1973;26:821–5.
[32] Lee DL, Powers JP, Pflegerl K, Vasil ML, Hancock RE, Hodges RS. Effects of single D-amino acid substitutions on disruption of beta-sheet structure and hydrophobicity in cyclic 14-residue antimicrobial peptide analogs related to gramicidin S. J Pept Res 2004;63:69–84.
[33] Ma B, Fang C, Zhang J, Wang MZ, Luo XX, Hou Z. Contemporaneous Measurement of Outer and Inner Membrane Permeability in Gram-negative Bacteria. Bio-Protocol 2020;10.
[34] Wenzel M, Vischer NOE, Strahl H, Hamoen LW. Assessing Membrane Fluidity and Visualizing Fluid Membrane Domains in Bacteria Using Fluorescent Membrane Dyes. Bio Protoc 2018;8:e3063.
[35] te Winkel JD, Gray DA, Seistrup KH, Hamoen LW, Strahl H. Analysis of Antimicrobial-Triggered Membrane Depolarization Using Voltage Sensitive Dyes. Front Cell. Dev Biol 2016;4.
[36] Dutta S, Watson B, Mattoon S, Rochet JC. Calcein Release Assay to Measure Membrane Permeabilization by Recombinant Alpha-Synuclein. Bio-Protocol 2020;10.
[37] Tang Y, Yang C, Liu CY, Xu YT, Peng MX, Chan EWC, et al. Development of an effective meropenem/KPC-2 inhibitor combination to combat infections caused by carbapenem-resistant *Klebsiella pneumoniae*. Int J Antimicrob Agents 2024;64.
[38] Hu TS, RamachandraRao SP, Siva S, Valancius C, Zhu YQ, Mahadev K, et al. Reactive oxygen species production via NADPH oxidase mediates TGF-β induced cytoskeletal alterations in endothelial cells. Am J Physiol-Renal 2005;289:F816–25.
[39] Kojima H, Nakatsubo N, Kikuchi K, Kawahara S, Kirino Y, Nagoshi H, et al. Detection and imaging of nitric oxide with novel fluorescent indicators: Diaminofluoresceins. Anal Chem 1998;70:2446–53.
[40] Setsukinai K, Urano Y, Kakinuma K, Majima HJ, Nagano T. Development of novel fluorescence probes that can reliably detect reactive oxygen species and distinguish specific species. J Biol Chem 2003;278:3170–5.
[41] Maeda T, Koch-Koerfges A, Bott M. Relevance of NADH Dehydrogenase and Alternative Two-Enzyme Systems for Growth of With Glucose, Lactate, and Acetate. Front Bioeng. Biotech 2021;8.
[42] Love MI, Huber W, Anders S. Moderated estimation of fold change and dispersion for RNA-seq data with DESeq2. Genome Biol 2014;15.
[43] Frisch MJ, Trucks GW, Schlegel HB, Scuseria GE, Robb MA, Cheeseman JR, et al. Gaussian 16 Rev. C.01. Wallingford, CT2016.
[44] Trubetskoy OV, Gibson JR, Marks BD. Highly miniaturized formats for in vitro drug metabolism assays using vivid fluorescent substrates and recombinant human cytochrome P450 enzymes. J Biomol Screen 2005;10:56–66.
[45] Vaara M. Agents That Increase the Permeability of the Outer-Membrane. Microbiol Rev 1992;56:395–411.
[46] Sanson A, Monck MA, Neumann JM. 2D 1H-NMR conformational study of phosphatidylserine diluted in perdeuterated dodecylphosphocholine micelles. Evidence for a pH-induced conformational transition. Biochemistry-Us. 1995;34:5938-44.
[47] French S, Puddephatt D, Habash M, Glasauer S. The dynamic nature of bacterial surfaces: Implications for metal-membrane interaction. Crit Rev Microbiol 2013;39:196–217.
[48] Pink DA, Hansen LT, Gill TA, Quinn BE, Jericho MH, Beveridge TJ. Divalent calcium ions inhibit the penetration of protamine through the polysaccharide brush of the outer membrane of Gram-negative bacteria. Langmuir 2003;19:8852–8.
[49] Dennison SR, Morton LHG, Harris F, Phoenix DA. Low pH Enhances the Action of Maximin H5 against and Helps Mediate Lysylated Phosphatidylglycerol-Induced Resistance. Biochemistry-Us 2016;55:3735–51.
[50] Epand RM, Epand RF. Bacterial membrane lipids in the action of antimicrobial agents. J Pept Sci 2011;17:298–305.
[51] Schieber M, Chandel NS. ROS Function in Redox Signaling and Oxidative Stress. Curr Biol 2014;24:R453–62.
[52] Mishra S, Imlay J. Why do bacteria use so many enzymes to scavenge hydrogen peroxide? Arch Biochem Biophys 2012;525:145–60.
[53] Vilchèze C, Weisbrod TR, Chen B, Kremer L, Hazbón MH, Wang F, et al. Altered NADH/NAD ratio mediates coresistance to isoniazid and ethionamide in mycobacteria. Antimicrob Agents Chemother 2005;49:708–20.

[54] Xie N, Zhang L, Gao W, Huang CH, Huber PE, Zhou XB, et al. NAD metabolism: pathophysiologic mechanisms and therapeutic potential. Signal Transduct Tar 2020;5.
[55] Feniouk BA, Suzuki T, Yoshida M. Regulatory interplay between proton motive force, ADP, phosphate, and subunit ε in bacterial ATP synthase. J Biol Chem 2007;282:764–72.
[56] Shukla R, Peoples AJ, Ludwig KC, Maity S, Derks MGN, Benedetti SD, et al. An antibiotic from an uncultured bacterium binds to an immutable target. Cell 2023;186.
[57] Zampaloni C, Mattei P, Bleicher K, Winther L, Thäte C, Bucher C, et al. A novel antibiotic class targeting the lipopolysaccharide transporter. Nature 2024;625.
[58] Song MR, Liu Y, Huang XY, Ding SY, Wang Y, Shen JZ, et al. A broad-spectrum antibiotic adjuvant reverses multidrug-resistant Gram-negative pathogens. Nature. Microbiology 2020;5:1040-+..
[59] Ahmed MAGES, Zhong LL, Shen C, Yang YQ, Doi Y, Tian GB. Colistin and its role in the Era of antibiotic resistance: an extended review (2000-2019). Emerg Microbes Infec 2020;9:868-85..
[60] Langton MJ, Serpell CJ, Beer PD. Anion Recognition in Water: Recent Advances from a Supramolecular and Macromolecular Perspective (vol 55, pg 4629, 2016). Angew Chem Int Edit. 2016;55:4629-.
[61] Murzyn K, Róg T, Pasenkiewicz-Gierula M. Phosphatidylethanolamine-phosphatidylglycerol bilayer as a model of the inner bacterial membrane. Biophys J 2005;88:1091–103.
[62] Nikolic P, Mudgil P. The Cell Wall, Cell Membrane and Virulence Factors of and Their Role in Antibiotic Resistance. Microorganisms 2023;11.
[63] Ramesh S, de la Torre BG, Albericio F, Kruger HG, Govender T. Microwave-Assisted Synthesis of Antimicrobial Peptides. Methods Mol Biol 2017;1548:51–9.
[64] Pedersen SL, Tofteng AP, Malik L, Jensen KJ. Microwave heating in solid-phase peptide synthesis. Chem Soc Rev 2012;41:1826–44.
[65] Hancock REW, Sahl HG. Antimicrobial and host-defense peptides as new anti-infective therapeutic strategies. Nat Biotechnol 2006;24:1551–7.
[66] Balli FN, Ekinci PB, Kurtaran M, Kara E, Dizman GT, Sönmezer MÇ, et al. Battle of polymyxin induced nephrotoxicity: Polymyxin B versus colistin. Int J Antimicrob Agents 2024;63.
[67] Nielsen M, Monberg T, Sundvold V, Albieri B, Hovgaard D, Petersen MM, et al. LTX-315 and adoptive cell therapy using tumor-infiltrating lymphocytes generate tumor specific T cells in patients with metastatic soft tissue sarcoma. Oncoimmunology 2024;13.
[68] Ciumac D, Gong HN, Hu XZ, Lu JR. Membrane targeting cationic antimicrobial peptides. J Colloid Interf Sci 2019;537:163–85.
[69] Bazzicalupi C, Bencini A, Giorgi C, Valtancoli B, Lippolis V, Perra A. Exploring the binding ability of polyammonium hosts for anionic substrates: selective size-dependent recognition of different phosphate anions by bis-macrocyclic receptors. Inorg Chem 2011;50:7202–16.
[70] Bianchi A, Giorgi C, Ruzza P, Toniolo C, Milner-White EJ. A synthetic hexapeptide designed to resemble a proteinaceous p-loop nest is shown to bind inorganic phosphate. Proteins 2012;80:1418–24.
[71] Denessiouk KA, Johnson MS, Denesyuk AI. Novel CalphaNN structural motif for protein recognition of phosphate ions. J Mol Biol 2005;345:611–29.